ACTA TECHNICA CORVINIENSIS – Bulletin of Engineering | e–ISSN: 2067 – 3809
Tome XIX [2026] | Fascicule 3 [July – September]

[1.]R. UMUNAKWE, [1.]A. O. OWOLAWI, [2.] I. J. UMUNAKWE, [3,4.]I. E. KALU,
[5.]W. U. EZE, [1.]Yemi AUDU, [6.]A. OYETUNJI

SILICA ENRICHMENT OF GRANITE MINE TAILINGS FROM SOUTHERN NIGERIA USING HYDROCHLORIC ACID LEACHING

[1.]Department of Materials and Metallurgical Engineering, Faculty of Engineering, Federal University Oye–Ekiti, Oye– Ekiti, Ekiti State, NIGERIA
[2.]Department of Chemistry, Faculty of Science, Federal University Oye–Ekiti, Oye– Ekiti, Ekiti State, NIGERIA
[3.]Physics Advanced Research Centre, Sheda Science and Technology Complex, Garki, Abuja, FCT, NIGERIA
[4.]Department of Civil Engineering, Walter Sisulu University, Buffalo City Campus, East London, 5200, SOUTH AFRICA
[5.]Polymer Technology Department, Nigerian Institute of Leather and Science Technology, Samaru–Zaria, Kaduna State, NIGERIA
[6.]Department of Metallurgical & Materials Engineering, School of Engineering & Engineering Technology, Federal University of Technology Akure, Ondo State, NIGERIA

Abstract: Granite mine tailings which are often regarded as waste contain valuable silicate minerals. Silica enrichment of the tailings can be achieved through chemical treatment. This study investigates the mineralogical transformation and silica enrichment potential of granite tailings from three mining locations in southern Nigeria. Hydrochloric acid (HCl) solution of different concentrations (3 M, 5 M, and 7 M) was utilized in the leaching process. The tailings were ball milled and sieved through British standard sieve sizes and the particles below 110 µm and above 75 µm was subjected to acid leaching under controlled conditions. The mine tailings samples before and after leaching were characterized using X–ray Diffraction (XRD) and Scanning Electron Microscopy with Energy Dispersive Spectroscopy (SEM–EDX). The XRD results revealed different leaching behaviors for the mine samples. Specifically, in samples from location 1 (L1), quartz became more prominent at 5 M HCl but was overtaken by anorthite as the dominant phase at 7 M. The behavior suggests recrystallization or selective retention of acid–resistant aluminosilicates. The samples obtained from location 2 (L2) showed progressive dissolution of phyllosilicates and feldspars as the acid concentration increased. Although anorthite dominated after 5 M HCl leaching, quartz became the major phase at 7 M. This indicates delayed but effective silica enrichment. In contrast, samples from location 3 (L3) retained complex feldspar and mica mineral even at high acid concentrations. The results show that effective silica recovery through acid leaching depends critically on the initial mineralogy of the tailings.
Keywords: Granite tailings, acid leaching, silica enrichment, mineralogical transformation

INTRODUCTION

Nigeria is blessed with different mineral resources that are present in all the 36 states (Fatoye, 2022). Mining activities are very predominant in Nigeria. Granite mining is very common in Nigeria. In 2006, It was reported that granite is in abundance in Ado-Ekiti and other southern part of Nigeria (Oyinloye and Obasi, 2006). Mining activities generate tailings in billions of tons on annual basis (Zhang at al., 2024). These tailings constitute environmental problems as they occupy space as solid wastes and pollute agricultural soils. Globally, conscious efforts are being made to recover materials from mining tailings. Recently, the properties tailing samples from quartz vein-hosted gold deposit and the possibility of recovering gold, feldspar, and quartz from the gold tailings by selective desliming, and flotation of gold bearing sulfide ore was reported (Chen at al., 2022). It has been reported that using 20 wt% activated granite tailings to replace cement significantly increased flexural strength and improved fracture resistance by lowering the compressive-to-flexural strength ratio (Hao at al., 2024). This was due to enhanced hydration and the interaction between cement products and oligomeric silica-alumina gels, which reduced matrix porosity and stabilized the structure (Hao at al., 2024). Reports exist on the recovery of silica from industrial wastes and mining tailings. A study grounded in the philosophy of environmental sustainability through resource recovery, aiming to reclaim high-purity silica from historical metallurgical tailings using a low-impact process (column flotation) rather than harsh chemicals or conventional waste disposal was presented [6]. Through a two-stage flotation column approach with optimized gas and liquid flow rates, the researchers achieved a 75.13% recovery of allotropic silica phases (quartz, tridymite, cristobalite) from “Dos Carlos” mining dam waste, producing a silica-rich concentrate suitable for ceramic and cement applications while minimizing feldspathic and metallic contaminants (Salinas-Rodriguez et al., 2020). Some researchers have recovered silicon and quartz from waste quartz crucible ash (WQCA) from monocrystalline silicon rod production through an innovative recovery process (Yang et al., 2024; Yang et al., 2024). A study has presented an environmentally friendly electrical separation process to recover

valuable silicon and quartz from quartz crucible waste ash (QCWA), a growing byproduct of monocrystalline silicon production (Yang et al., 2024). Through theoretical force analysis, simulations, and experiments, the process achieved over 93% silicon content in the concentrate and more than 61% quartz content in the tailings, demonstrating an efficient and scalable method for resource recovery from PV manufacturing waste (Yang et al., 2024). Further, using a combination of electric separation and sequential acid-alkaline leaching, followed by vacuum induction refining, the study successfully produced high-purity silicon (20.8 ppmw impurity) and quartz (98.15% purity), demonstrating a viable path for converting PV waste into valuable industrial materials (Yang et al., 2024). Another study also presented a novel two-step method combining Superconducting High Gradient Magnetic Separation (S-HGMS) with acid (mixtures of HCl, H2SO4, and HNO3 acids) leaching to efficiently recover and purify high-grade silica (99.51% SiO_2) from high-silicon iron ore tailings (IoTs), addressing environmental concerns and enabling resource reus (Li et al., 2023). In another report, S-HGMS was used to achieve an initial silica concentration of 92.06% from high silicon IoTs which was further refined to 99.51% purity through optimized mixed acid (5 mol/L HCl + 1 mol/L HF) leaching, demonstrating an efficient and sustainable route for transforming waste into valuable industrial material (Li et al., 2023). Attention has been given to the recovery of resources from granite-type sulfide mine tailings. A study embraced the philosophy of sustainable resource utilization by recovering valuable non-metallic minerals (mica and quartz) from granite-type sulfide mine tailings without using acid, aligning with China's green mining initiative to minimize environmental impact and reduce tailings stockpile (Zhang et al., 2024). Through sequential flotation experiments—removing pyrite first, followed by desliming and mechanical separation at optimized pH (10.3), pulp concentration (35%), and collector dosage (180 g/t)—the authors achieved recoveries of 12.89% mica and 42.73% quartz (71.5% SiO_2), producing marketable products for construction applications (Zhang et al., 2024). In this work, the possibility of silica recovery through acid leaching from granite-type mine tailings obtained from three mine locations in Ekiti and Edo states in Nigeria is presented.

MATERIALS AND METHODS

Materials Preparation

The dry tailings samples used for the experiment were collected from three granite mining sites located in the southern region of Nigeria. These sites are; Location 1 (GPS location 6°43'41''N 5°11'5''E) (Edo State), Location 2 (GPS location 7°42'17''N 5°16'3''E) (Iworoko, Ekiti State), and Location 3 (GPS location 7°40'52''N 5°10'49''E) (Iyin, Ekiti State). Each sample was milled using a Denver ball mill to homogenize the material and reduce the particle sizes. The samples were then sun-dried and sieved using a sieve shaker fitted with British Standard (BS) sieves. Four sieve sizes were employed: 53 µm, 63 µm, 75 µm, and 110 µm resulting in the collection of four particle size fractions: +110 µm, +75 µm –110 µm, +63 µm –75 µm, and +53 µm –63 µm. The +75 µm –110 µm fraction was selected for subsequent experimental work. Samples codes for the collected samples are presented in Table 1 for identification and reporting purposes.

Table 1. Sample codes of the tailing samples

Sample code for location 1 (L1)	L1– BL	L1– 3ML	L1– 5ML	L1–7ML
Code description of L1 samples	Before leaching	After leaching with 3 M HCl	After leaching with 5 M HCl	After leaching with 7 M HCl
Sample code for location 2 (L2)	L2– BL	L2– 3ML	L2– 5ML	L2–7ML
Code description of L2 samples	Before leaching	After leaching with 3 M HCl	After leaching with 5 M HCl	After leaching with 7 M HCl
Sample code for location 3 (L3)	L3– BL	L3– 3ML	L3– 5ML	L3–7ML
Code description of L3 samples	Before leaching	After leaching with 3 M HCl	After leaching with 5 M HCl	After leaching with 7 M HCl

Leaching with Hydrochloric Acid

Leaching experiments were conducted using the sieved tailings samples with a particle size of +75 µm –110 µm using hydrochloric acid (HCl) at concentrations of 3 M, 5 M, and 7 M. 20 g of each sample measured with a sensitive digital weighing balance was used for each experiment. The leaching process was carried out using a magnetic stirrer for 60 minutes. The leaching parameters were a solid-to-liquid ratio of 1:20, a temperature of 80°C, and a stirring speed of 300 rpm. After leaching, the samples were filtered using Whatman grade 42 filter paper after leaching, thoroughly washed with distilled water, and dried in an electric oven at 110°C for 2 hours to prepare them for further analysis. The dried samples were weighed to estimate the yield percentage relative to the initial 20 g before leaching. The use of HCl for the leaching is based on earlier reports that 0.5 - 9.6 M HCl have been reported to effectively dissolve other minerals such as iron, aluminum, carbonates, feldspars, and clay-rich phases while leaving quartz relatively unaffected due to its strong Si-O bonding (Amin et al., 2020; Lashen et al., 2016).

Characterization of the Samples

The chemical and mineralogical compositions of the raw and leached tailings samples were characterized using scanning electron microscopy and x-ray diffraction. A high-resolution Scanning Electron Microscope equipped with Energy Dispersive X-ray spectroscopy (SEM-EDX) (Phenom ProX Desktop SEM, ThermoFisher Scientific, USA) was used to examine the morphology and elemental composition of the tailings samples from the three locations before and after leaching with 5 M HCl. Before imaging, the powder samples were mounted on stubs using double-sided adhesive tape and sputter-coated with a 5 nm layer of gold to enhance conductivity using an auto coater (Q150R Plus, Quorum Technologies, England). SEM imaging was carried out at an accelerating voltage of 15 kV and a magnification of ×1500.

A benchtop X-ray Diffractometer (Rigaku MiniFlex 600, Japan) was employed to identify the mineral phases present and their amounts in each of the prepared tailing sample before and after leaching over a 2θ range of 10° to 70°.

RESULTS AND DISCUSSION

Physical Appearance of the Tailing Samples Before and After Leaching

The camera images of the milled and sieved tailings samples from the three locations before and after leaching with 3 M, 5 M, and 7 M HCl are shown in Figure 1. The tailings before leaching appeared relatively coarse, granular, and compact. Some dark mineral inclusions were seen. After leching, they appeared whiter. Acid leaching resulted in the dissolution of acid-soluble minerals, removal of impurities and reduction of granularity. Whiter and finer products, which have the potentials for applications in the ceramics industry, and as construction filler were obtained.

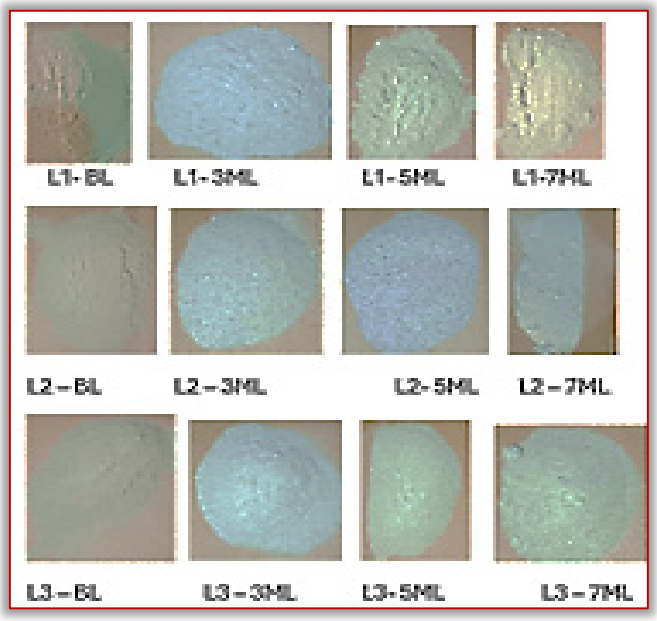

Figure 1. Photo images of the tailings from different locations before and after leching with different HCl concentrations

Percentage Yield of the Residue After Leaching

Figure 2 shows the percentage yield of residue mass after leaching the granite tailings from three mine locations. The trend was not uniform across the three locations, indicating that the tailings from different locations have distinct initial mineralogical compositions and reactivities to acid. The leaching efficiency and resulting yield were observed to be influenced by both acid concentration and the inherent mineralogy of the tailings. Sample L1 showed a U-shaped yield profile, possibly due to intermediate leaching (5 M HCl) dissolving more loosely bound materials, and higher molarity (7 M HCl) stabilizing silica-rich phases in the residue. Sample L2 exhibited a typical leaching behavior where higher acid concentration dissolves more material, lowering solid yield. Sample L3 showed a positive response to higher acid concentrations, which could be due to strong removal of coatings, exposing the core of the more stable silica-rich phases. The ideal leaching condition granite tailings from different locations will therefore depend on the mineralogy of the tailings. Generally, the results show that hydrochloric acid selectively dissolves metal oxides but does not disrupt quartz structures, explaining the enrichment in Si-rich phases. This is consistent with Zhang et al. (2023), who noted that HCl effectively removes impurities while leaving quartz largely unaffected.

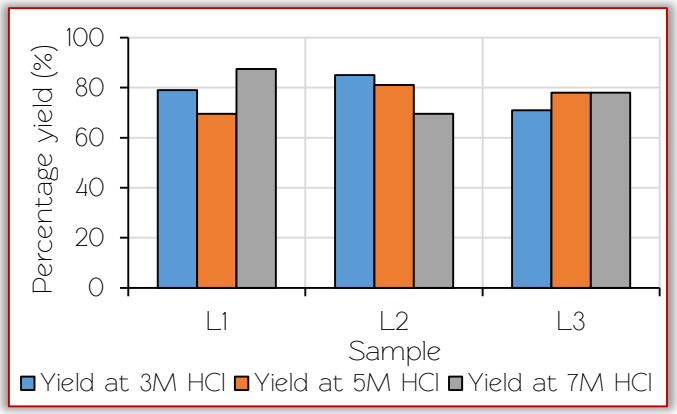

Figure 2. Percentage yield of the residue after leaching

Morphological and Elemental Evolution Of Granite Tailings and Its Correlation with Leaching Yield

The SEM and EDX analyses provided vital insights into the morphological and compositional transformations of the granite tailing samples L1, L2, and L3 before and after acid leaching with 5 M HCl. The findings were observed to closely correlate with the observed percentage yield of the solid residues. The SEM micrograph of sample L1-BL shown in Figure 3 (a) revealed a heterogeneous structure. The grains were found to be irregular, compact, and exhibit rough surface

texture, suggestive of significant contamination by mineral inclusions.

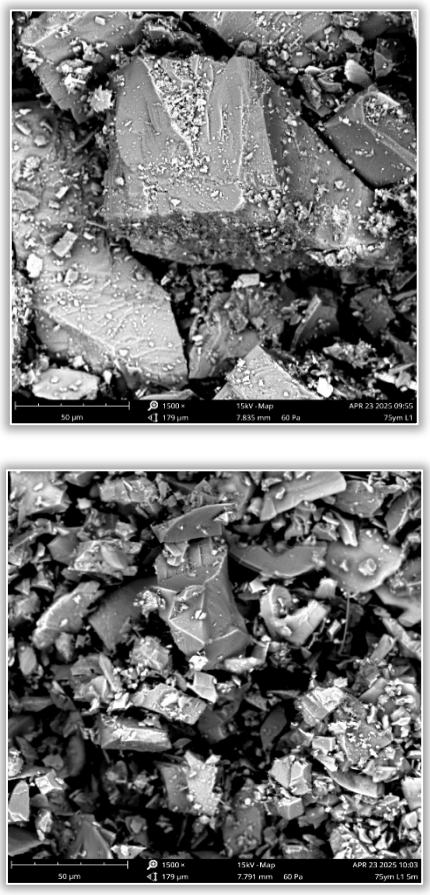

Figure 3. SEM micrographs of the granite tailings at 50 µm scale, before and after leaching (a) for sample L1–BL and (b) for sample L1–5ML

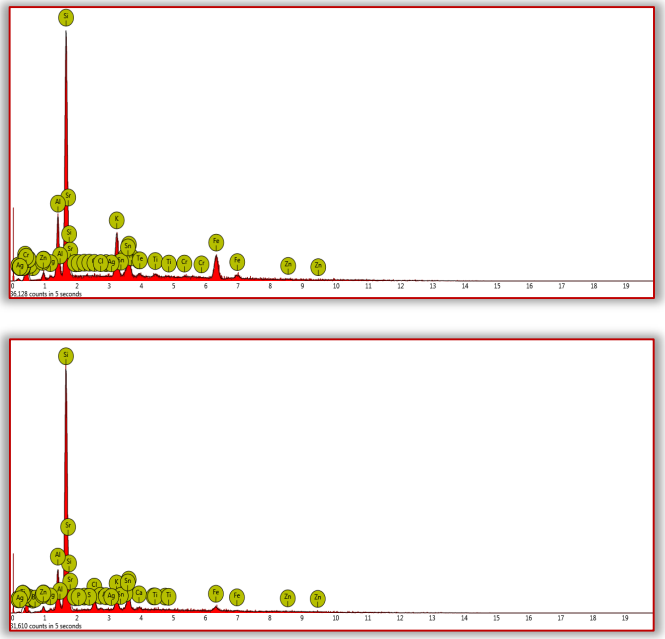

Figure 4. EDX spectra of the granite tailings, before and after leaching (a) for sample L1–BL and (b) for sample L1–5ML

The EDX spectrum of sample L1-BL shown in Figure 4 (a) and presented in Table 2 confirmed the presence of various acid-soluble impurities, including Fe (23.38 wt%), Ca (5.19 wt%), Sr (7.71 wt%), and Zn (2.68 wt%), with a silicon content of 35.26 wt%.

Table 2. Elemental composition of L1–BL and L1–5ML

Element		Si	Fe	K	Al	Sr	Ca	Zn	Te
Weight conc (%)	L1–BL	35.26	23.38	10.77	8.53	7.71	5.19	2.68	2.67
	L1–5ML	51.14	6.84	5.97	7.76	13.21	8.52	–	–

Element		Na	Ti	Sn	Mg	Cl	S	Total
Weight conc (%)	L1–BL	1.39	1.07	1.05	0.3	–	–	100
	L1–5ML	0.91	–	1.44	0.25	3.84	0.12	100

After leaching with 5 M HCl (L1-5ML), the SEM micrograph presented in Figure 3 (b) revealed noticeable surface refinement, reduced agglomeration, and improved definition of grain boundaries. This shows that loosely bound impurities were effectively dissolved. EDX analysis presented in Figure 4 (b) and Table 2 supported these observations, as silicon concentration rose sharply to 51.14 wt%, while iron and other impurity significantly reduced. Interestingly, the yield profile for L1 shown in Figure 2 exhibited a U-shaped trend, where the residue mass initially decreased at 5 M HCl indicating maximum impurity removal, and then slightly increased at 7 M. This suggested that while moderate acid concentration (5 M) optimally removed soluble phases, higher concentrations may have promoted the stabilization of residual silica-rich frameworks or resulted in the formation of secondary non-soluble residues, such as reprecipitated gels or salt complexes.

The SEM image of sample L2-BL shown in Figure 5 (a) displayed a dense and compact morphology, with fine mineral phases heavily present on the surfaces. EDX analysis presented in Figure 6 (a) and Table 3 indicated a complex elemental profile. This includes high levels of Fe (26.93 wt%), Ca (7.48 wt%), Sr (6.57 wt%), and Al (10.78 wt%), and an initial silicon content of 39.84 wt%.

After leaching (L2-5ML), a dramatic morphological transformation occurred: the SEM micrograph depicted in Figure 5 (b) showed a markedly cleaner and more porous structure, signifying thorough dissolution of superficial coatings and deeper exposure of the silica matrix. This was corroborated by EDX results presented in Figure 6 (b) and Table 3, showing a pronounced increase in silicon to 62.33 wt%—the highest among all samples—and a substantial reduction in Fe, Ca, and Al concentrations. The yield trend for L2, as shown in Figure 2, exhibited a continuous decline with increasing acid concentration. This is the characteristic of a typical leaching profile where

mass loss directly corresponds to the removal of soluble phases. The high silica enrichment and advanced morphological cleaning is an indication that the tailings from L2 were highly reactive to acid and well-suited for silica recovery using hydrochloric acid leaching.

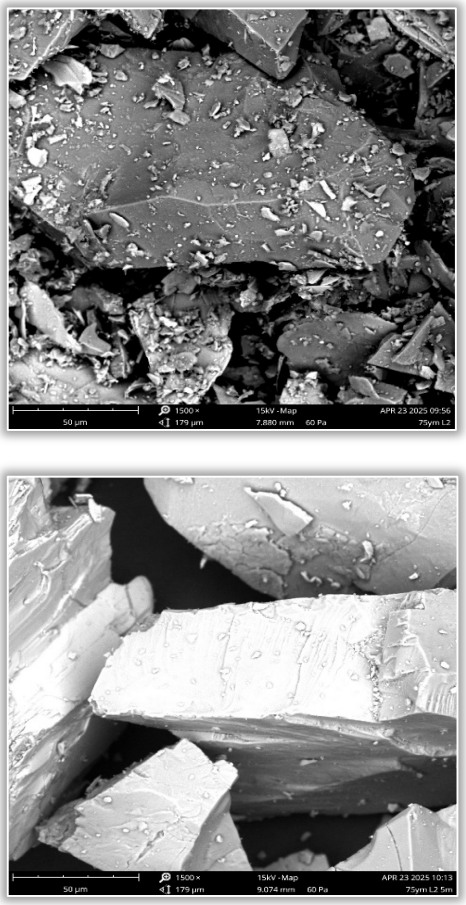

Figure 5. SEM micrographs of the granite tailings at 50 µm scale, before and after leaching (a) for sample L2–BL (b) for L2–5ML

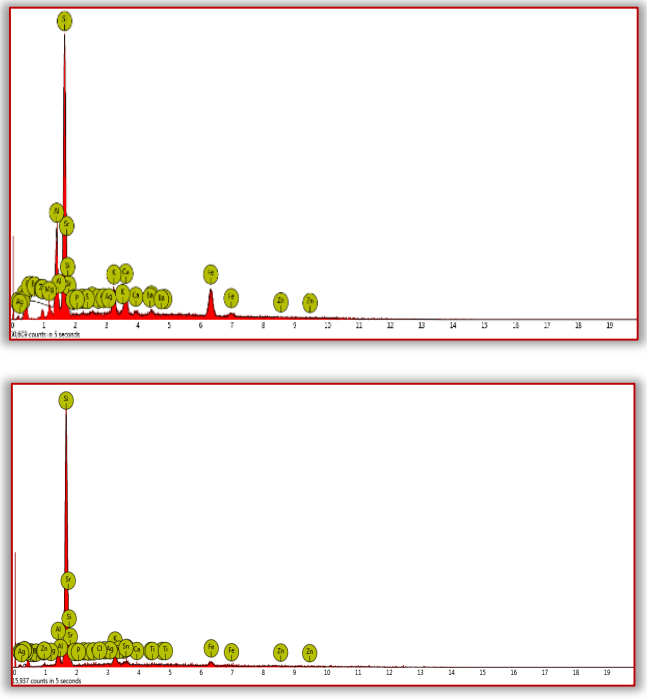

Figure 6. EDX spectra of the granite tailings, before and after leaching (a) for sample L2–BL (b) for sample L2–5ML

Table 3. Elemental composition of L2–BL and L2–5ML

Element		Si	Fe	Al	Ca	Sr	K	Ti	Cl
Weight conc (%)	L2–BL	39.84	26.93	10.78	7.48	6.57	6.01	0.46	0.46
	L2–5ML	62.33	8.05	4.64	1.64	14.65	5.49	–	–

Element		S	Sn	Na	Total
Weight conc (%)	L2–BL	0.14	–	–	100
	L2–5ML	0.18	2.56	0.46	100

In contrast, the tailing sample L3 showed a less pronounced response to acid leaching. The SEM image of L3-BL shown in Figure 7 (a) displayed an agglomerated, rough-textured surface with darker regions indicative of embedded metal oxides and clay-rich phases.

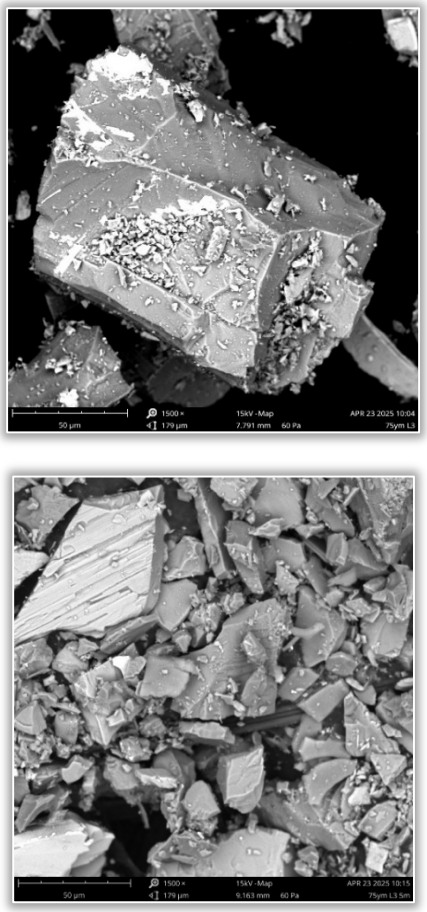

Figure 7. SEM micrographs of the granite tailings at 50 µm scale, before and after leaching (a) for sample L3–BL and (b) for sample L3–5ML

The EDX data presented in Figure 8 (a) and Table 4 indicated a relatively higher starting silicon content (44.15 wt%) but also significant quantities of Fe (18.05 wt%), Sr (11.59 wt%), and Al (11.13 wt%). After treatment with 5 M HCl (L3-5ML), the surface morphology depicted in Figure 7 (b) exhibited only moderate cleaning, with residual

agglomerations still visible, indicating incomplete leaching or poor accessibility of internal mineral phases. Correspondingly, EDX analysis showcased in Figure 8 (b) and Table 4 revealed only a modest increase in silicon content to 49.31 wt%, while notable amounts of Fe (8.28 wt%), Sr (10.99 wt%), and Al (9.41 wt%) persisted. Interestingly, the yield of solid residue for L3, as shown in Figure 2 increased with acid concentration—a trend contrary to L2—suggesting that leaching preferentially removed external, loosely attached impurities without penetrating or dissolving deeper, possibly encapsulated phases. The increase in yield may be an indication of the formation of stable, acid-resistant silicate frameworks or the exposure of inert quartz-rich cores that contribute more mass post-leaching.

Table 4. Elemental composition of L3–BL and L3–5ML

Element		Si	Fe	Sr	Al	Ca	K	Na	Ti
Weight conc (%)	L3–BL	44.15	18.05	11.59	11.13	6.73	6.30	0.73	0.49
	L3–5ML	49.31	8.28	10.99	9.41	8.7	7.30	0.88	1.03

Element		S	Cl	Mg	Zn	Ag	Total
Weight conc (%)	L3–BL	0.34	0.28	0.21	–	–	100
	L3–5ML	–	1.48	0.14	1.87	0.61	100

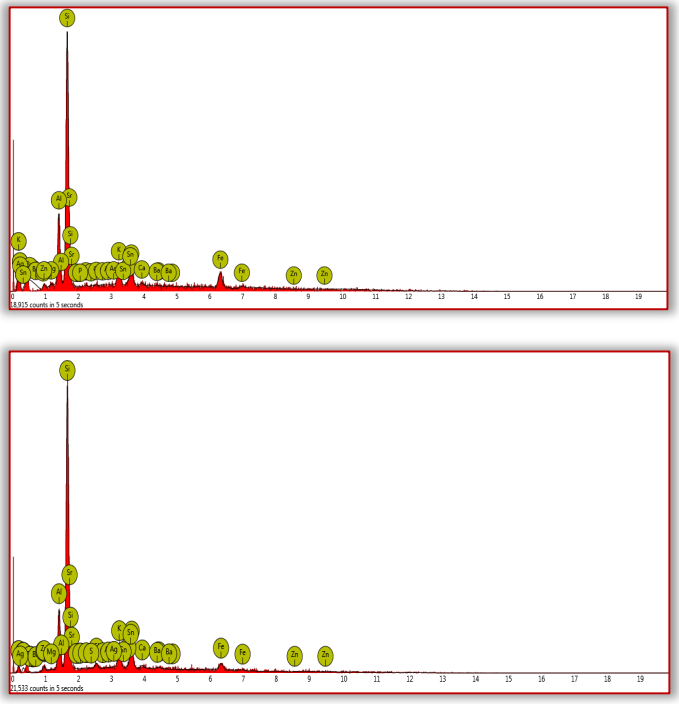

Figure 8. EDX spectra of the granite tailings, before and after leaching (a) for sample L3–BL and (b) for sample L3–5ML

The emergence of trace sulfur (S) detected by EDX was also observed across the leached samples, despite hydrochloric acid containing no sulfur. This suggests that the sulfur originated from the native mineral composition of the tailings, likely from sulfide minerals such as pyrite (FeS_2) or chalcopyrite ($CuFeS_2$). These minerals were partially exposed or dissolved during leaching. The detection of residual chlorine (Cl) in the post-leach samples is as a result of the retention of leaching-derived ions, possibly as adsorbed species or in the form of salt precipitates.

Collectively, the SEM-EDX findings correlate well with the yield data. The findings highlight the different reactivities of the tailings from each location. The L2 samples, which exhibited the most significant yield reduction, also displayed the highest silica purity and the most pronounced morphological improvement, signifying efficient leaching. L1 followed with intermediate behavior, showing high silica enrichment at 5 M HCl and a non-linear yield trend. In contrast, L3 showed the least response to acid leaching, both in terms of yield reduction and silica purification, indicating a more refractory or encapsulated mineral structure. These differences point towards the need to tailor leaching parameters to the mineralogical characteristics of the tailings for effective silica recovery. The progressive increase in Si content with higher HCl molarity for samples L1and L2 is an indication that stronger acidic conditions facilitate the selective removal of feldspars and mica, leading to high-silica residues. Similar enrichment trend was observed in granite quarry waste leached using varying HCl concentrations, where SiO_2 purity rose from 62 % to 73 % at ~10 M HCl (Long at al., 2025).

The limited response of L3 to HCl leaching arises from its mineralogy, dominated by muscovite, biotite, alkali feldspars, and illite, all of which form structurally resilient aluminosilicate frameworks. Micas, with their strongly bonded octahedral-tetrahedral layers, resist proton attack more than smectite clays or Na/K-feldspars. L3 also contains higher initial Si and notable Fe/Mg incorporation in its silicate lattices, producing acid-resistant complexes that slow dissolution and restrict silica release. The appearance of secondary phases such as topaz and biotite after leaching indicates structural reorganization rather than full breakdown, further reducing acid-treatment effectiveness.

Crystalline Phase Changes in the Granite Tailings and Their Relationship with Morphology and Acid Leaching Behaviour

The XRD analysis of granite tailings from three mine locations (L1, L2, and L3) before and after leaching with hydrochloric acid reveals significant trends in mineralogical transformation. The results provide insight into the behavior of individual phases under chemical treatment. There is a close correlation between the transformations observed

by XRD and both the morphological evolution observed by SEM and the elemental profiles identified through EDX analysis was observed in granite quarry waste leached using varying HCl concentrations, where SiO_2 purity rose from 62 % to 73 % at ~10 M HCl [16].

L1 Samples: Acid-Induced Redistribution Favoring Anorthite at High Molarity

The XRD pattern of the untreated sample L1-BL, shown in Figure 9 (a) with the mineralogical counts in Figure 9 (b), revealed a diverse mineralogy dominated by orthoclase ($KAlSi_3O_8$), albite ($NaAlSi_3O_8$), anorthite ($CaAl_2Si_2O_8$), muscovite ($KAl_2(AlSi_3O_{10})(OH)_2$), and quartz ($SiO_2$). This complex feldspathic and mica-bearing assemblage explains the significant presence of Al, K, Ca, Na, and Fe observed in the EDX profile (Table 2).

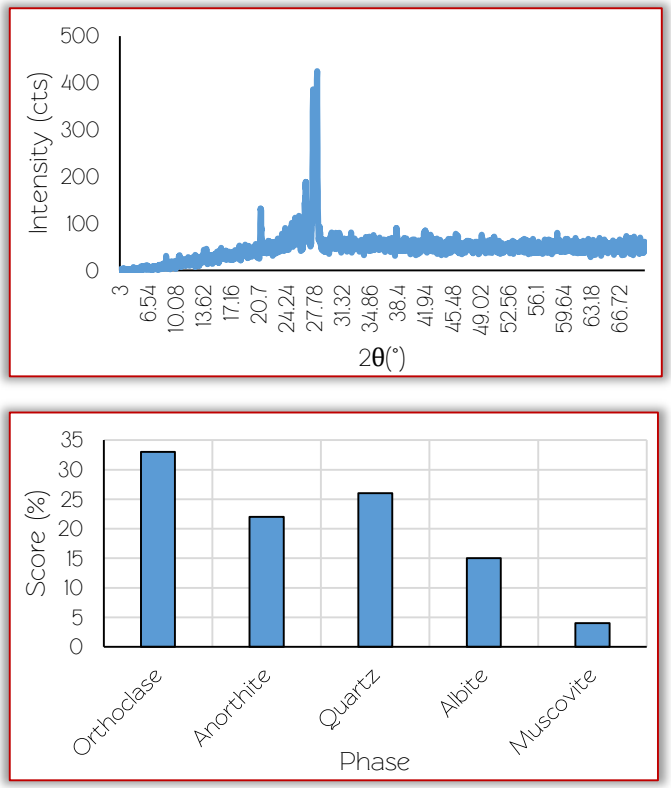

Figure 9. Granite tailings (before leaching): Sample L1–BL (a) XRD pattern and (b) phases and their scores

After leaching with 3 M and 5 M HCl (Figures 10 (a) and 11 (a)), XRD patterns showed a general reduction in the intensity of orthoclase and albite peaks, reflecting the preferential dissolution of these acid-soluble feldspars, as presented in Figures 10 (b) and 11 (b). Concurrently, quartz peaks became more prominent, suggesting the relative concentration of acid-insoluble silica. This trend aligns with SEM observations showing surface cleaning and grain boundary refinement, and with EDX data revealing reduced impurity concentrations and a peak in silicon content at 5 M HCl. However, at 7 M HCl (Figure 12 (a)), a notable shift occurred: anorthite emerged as the dominant crystalline phase, surpassing quartz in peak intensity, as presented in Figure 12 (b). This suggests that under stronger acid conditions, either anorthite persisted while other feldspars and quartz dissolved; or became structurally altered or crystallized or reorganized from the breakdown of more soluble feldspars such as albite and orthoclase, forming a more acid-resistant framework.

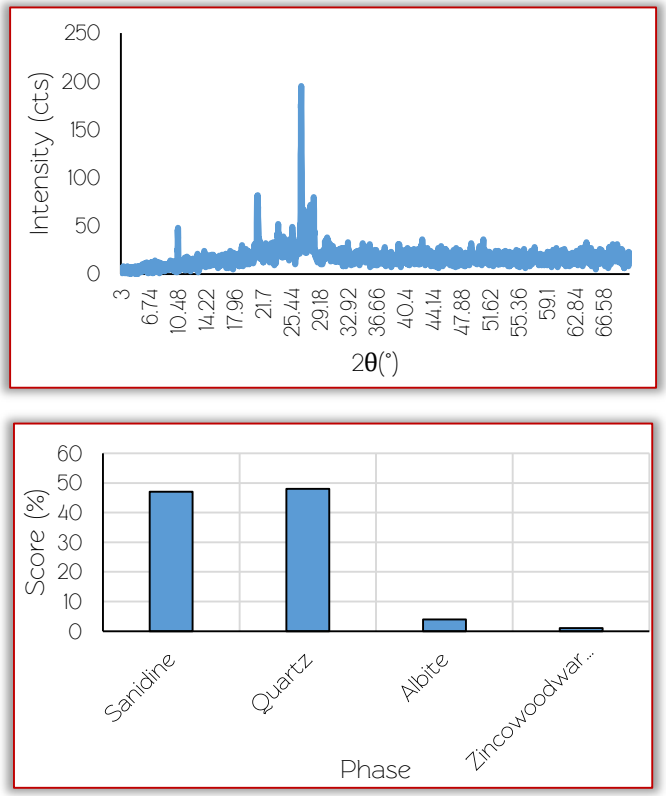

Figure 10. Granite tailings (after leaching): Sample L1–3ML (a) XRD pattern and (b) phases and their scores

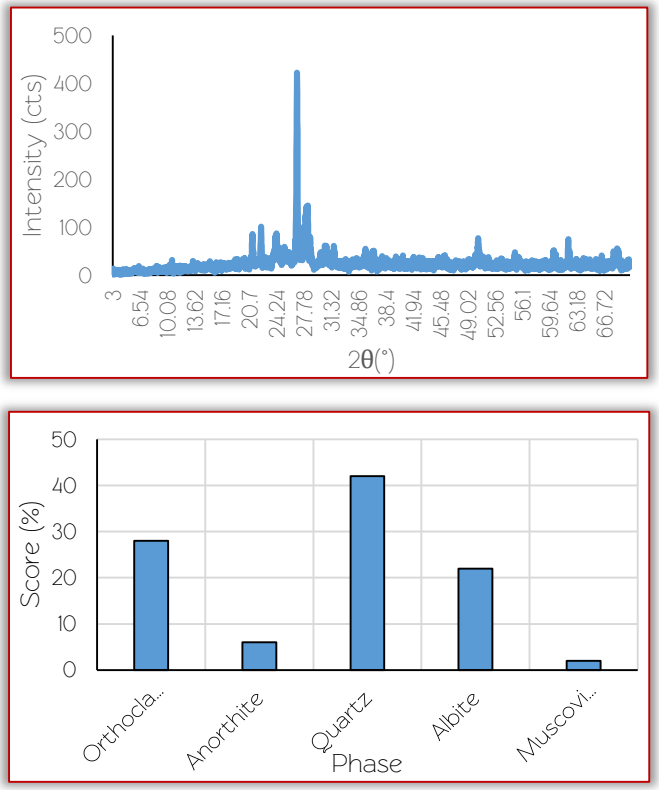

Figure 11. Granite tailings (after leaching): Sample L1–5ML (a) XRD pattern and (b) phases and their scores

This reorganization may reflect a complex chemical equilibrium at higher acid molarities, where dissolution and reprecipitation occur simultaneously, producing a mineral residue richer in calcium aluminosilicates such as anorthite.

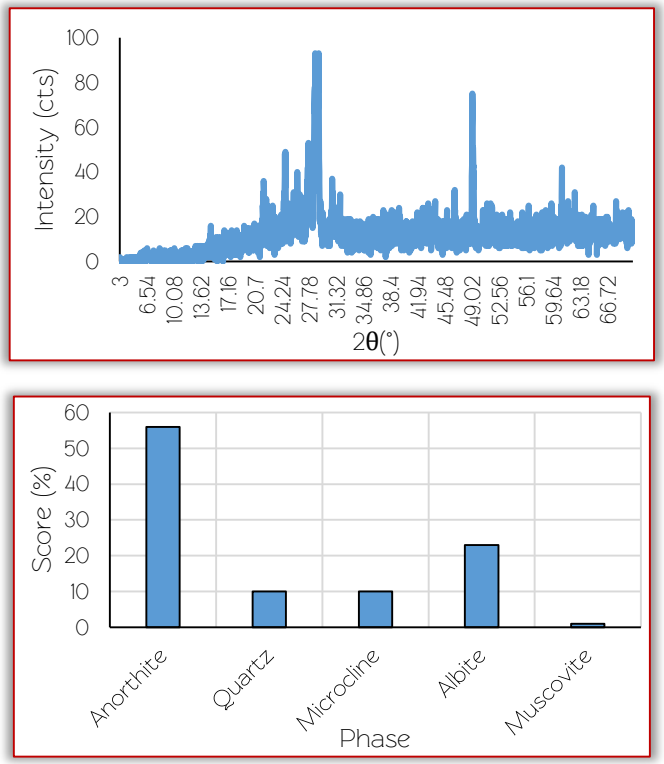

Figure 12. Granite tailings (after leaching): Sample L1–7ML (a) XRD pattern and (b) phases and their scores

L2 Samples: Removal of Layered Silicates and Feldspars Leads to Quartz Enrichment

The XRD pattern of the tailing sample L2-BL (Figure 13 (a)) revealed a complex mineral assemblage, with predominant phases presented in Figure 13 (b) identified as:

- Phlogopite-1M [$KMg_3(AlSi_3O_{10})(OH)_2$], a mica-group mineral containing potassium, magnesium, and aluminum;
- Montmorillonite [$Na_{0.33}(Al,Mg)_2Si_4O_{10}(OH)_2 \cdot nH_2O$], a swelling clay mineral in the smectite group;
- Quartz [SiO_2], a chemically resistant framework silicate; Illite [$K_{0.65}Al_{2.0}(Al_{0.65}Si_{3.35}O_{10})(OH)_2$], a non-expanding mica-like clay;
- Orthoclase [$KAlSi_3O_8$], a potassium feldspar; and Albite [$NaAlSi_3O_8$], a sodium feldspar.

This mineralogical diversity aligns with the rich chemical profile observed in EDX (Table 3), including high levels of Al, K, Mg, Na, and Fe, with a moderate initial silicon content of 39.84 wt%. After leaching with 3 M and 5 M HCl (Figures 14 (a) and 15 (a), there was a marked reduction in peak intensities associated with phlogopite, montmorillonite, illite, orthoclase, and albite, as shown in the counts presented in Figures 14 (b) and 15 (b)). This implies that these layered silicates and feldspars were susceptible to acid attack. As these phases were progressively dissolved, quartz (SiO_2) became the dominant residual phase due to its highly resistance to acid dissolution. The XRD pattern of the sample leached with 5 M HCl (Figures 15 (a) and 15 (b)) revealed a substantial loss of mica and clay mineral peaks, particularly those associated with phlogopite, montmorillonite, and illite, indicating their preferential dissolution.

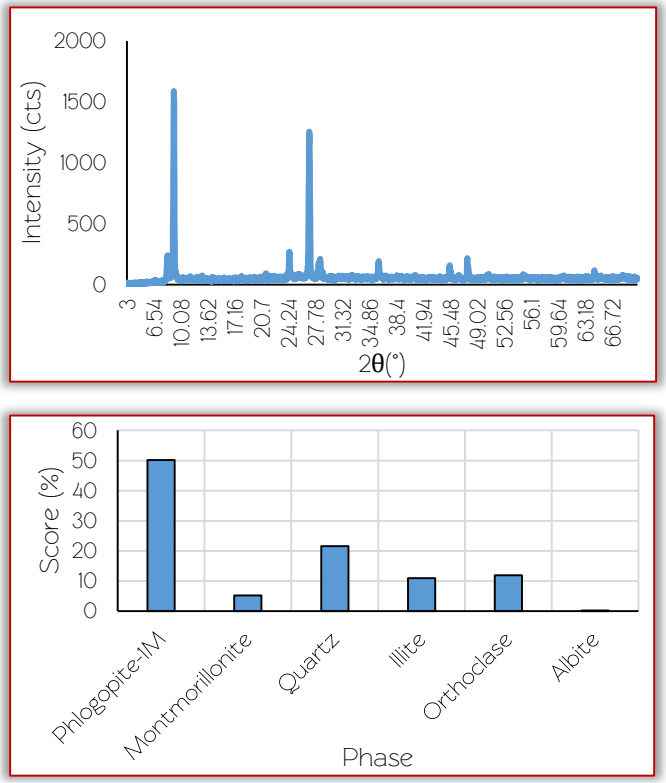

Figure 13. Granite tailings (before leaching): Sample L2–BL (a) XRD pattern and (b) phases and their scores

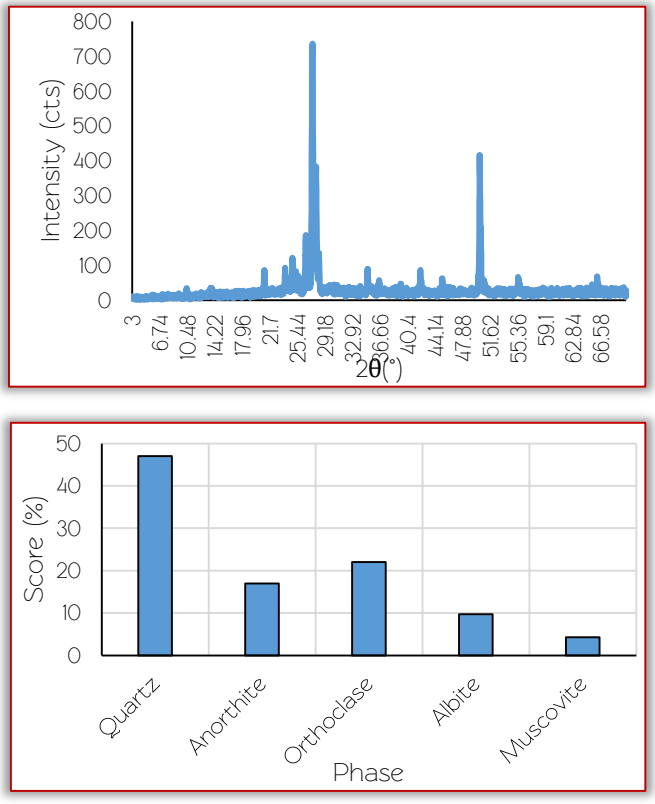

Figure 14. Granite tailings (after leaching): Sample L2–3ML (a) XRD pattern and (b) phases and their scores

Feldspar phases also showed marked reduction—except for anorthite [$CaAl_2Si_2O_8$], which emerged as the most predominant crystalline phase after leaching. This dominance of anorthite over quartz post-leaching could be as a result of the selective dissolution of more soluble phases, such as Na/K-rich feldspars (albite, orthoclase) and expandable clays, which left behind the more acid-resistant Ca-rich feldspar, anorthite; or reorganization or recrystallization, wherein residual Al and Ca, released from feldspars and clays during leaching, reprecipitated into structurally stable anorthite under the leaching conditions.

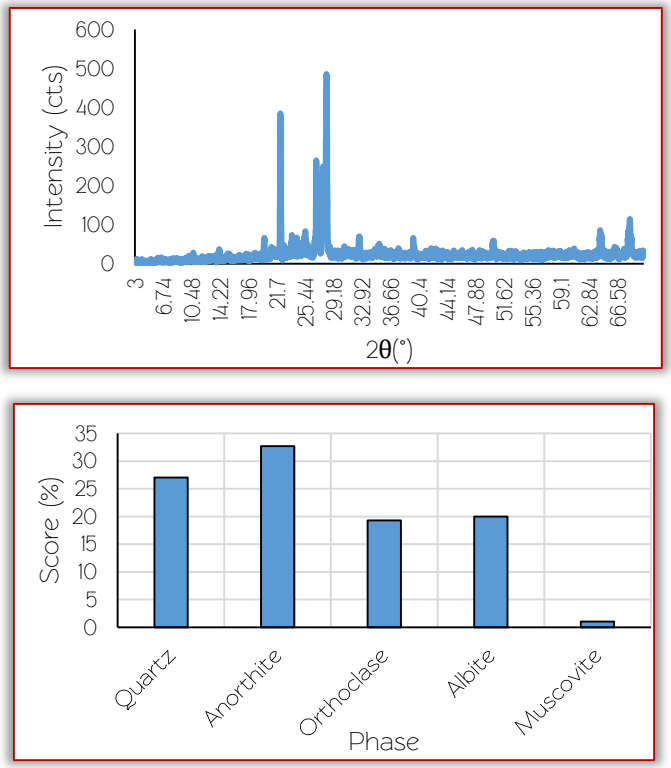

Figure 15. Granite tailings (after leaching): Sample L2–5ML (a) XRD pattern and (b) phases and their scores

The SEM image of L2-5ML (Figure 5 (b)) showed a markedly cleaner and more porous texture, consistent with substantial mineral breakdown and dissolution. Meanwhile, EDX analysis (Table 3) revealed a high silicon concentration (62.33 wt%) and reduced Al, Fe, Ca, and Sr content, indicating a net purification of the solid. However, the persistence and dominance of anorthite in the XRD pattern highlight that the residue is composed primarily of an acid-stable calcium aluminosilicate framework, and not pure silica (quartz). This contrasts with the conventional expectation that quartz becomes dominant following acid purification. In this case, anorthite resists dissolution more effectively than other feldspars and clays, making it the major survivor of acid leaching in L2. The yield trend (Figure 2) supports this, as mass loss continued up to 5 M HCl, corresponding to the removal of acid-soluble phases and stabilization of more resilient anorthite-rich residues. When leached with 7 M HCl (Figures 16 (a) and 16 (b)), quartz peaks became more dominant relative to anorthite, indicating further dissolution of remaining aluminosilicates, including anorthite, and enrichment of the silica fraction.

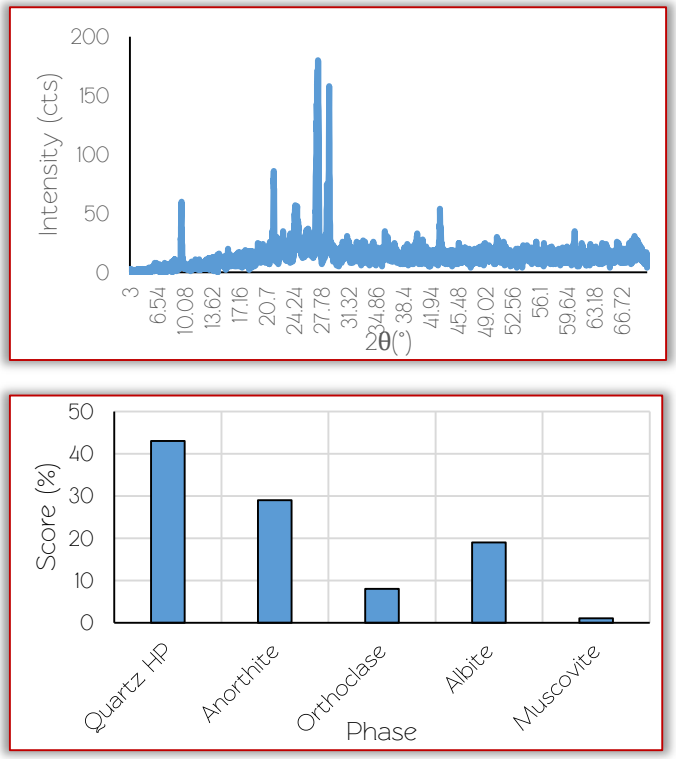

Figure 16. Granite tailings (after leaching): Sample L2–7ML (a) XRD pattern and (b) phases and their scores

L3 Samples: Progressive Phase Transition with Persistent Silicate Complexity

The XRD pattern of the untreated tailing sample L3-BL (Figures 17 (a) and 17 (b)) reveals a mica- and clay-rich mineralogy, dominated by: Illite [$K_{0.65}Al_{2.0}(Al_{0.65}Si_{3.35}O_{10})(OH)_2$], a non-expanding clay mineral in the mica group; Muscovite-2M1 [$KAl_2(AlSi_3O_{10})(OH)_2$], a well-ordered dioctahedral mica; Orthoclase [$KAlSi_3O_8$] and Albite [$NaAlSi_3O_8$], representing potassium and sodium feldspars, respectively; Quartz [SiO_2], a chemically inert framework silicate, present in moderate amounts; A small amount of Montmorillonite [$Na_{0.33}(Al,Mg)_2Si_4O_{10}(OH)_2 \cdot nH_2O$], a smectite-type swelling clay. This reflects a typical weathered granite tailing containing layered aluminosilicates and feldspars, supported by the presence of Al, K, Fe, and Si in the EDX data (Table 4). Morphologically, the L3-BL SEM image (Figure 7 (a)) showed compact, irregular grains with fine agglomerations—typical of clay-mineral-bearing systems.

Leaching with 3 M HCl resulted in a moderate shift in the mineralogy. The XRD pattern (Figures 18 (a) and 18 (b)) showed a decrease in illite and montmorillonite—typical acid-reactive clays—but retained a diverse mix of feldspar and mica-group phases, including: Quartz (SiO_2), albite ($NaAlSi_3O_8$), sanidine ($K(AlSi_3O_8)$), anorthite ($CaAl_2Si_2O_8$), and

muscovite ($KAl_2(AlSi_3O_{10})(OH)_2$). Quartz was more pronounced than in L3-BL but not dominant, suggesting relative enrichment through partial removal of acid-soluble phases rather than full purification. The continued presence of alkali feldspars and muscovite points to limited acid efficacy at this stage.

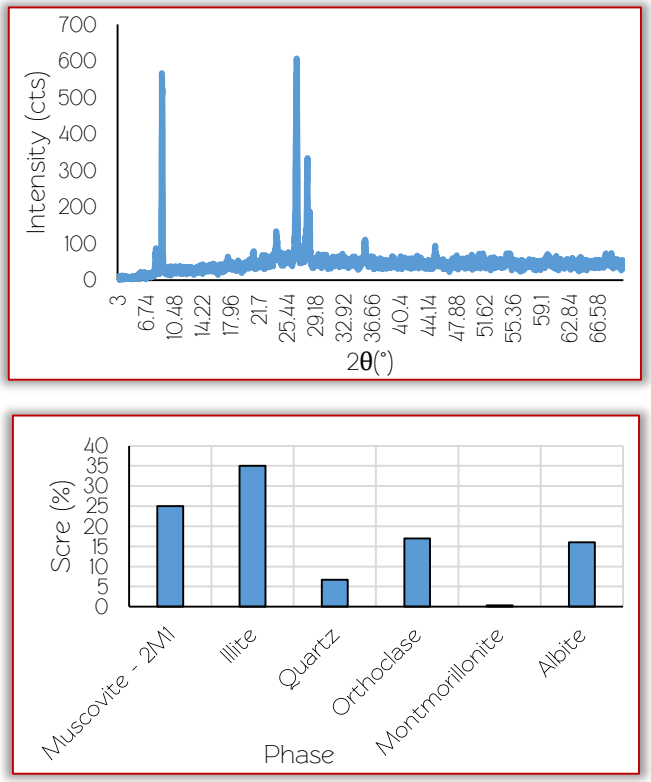

Figure 17. Granite tailings (before leaching): Sample L3–BL (a) XRD pattern and (b) phases and their scores

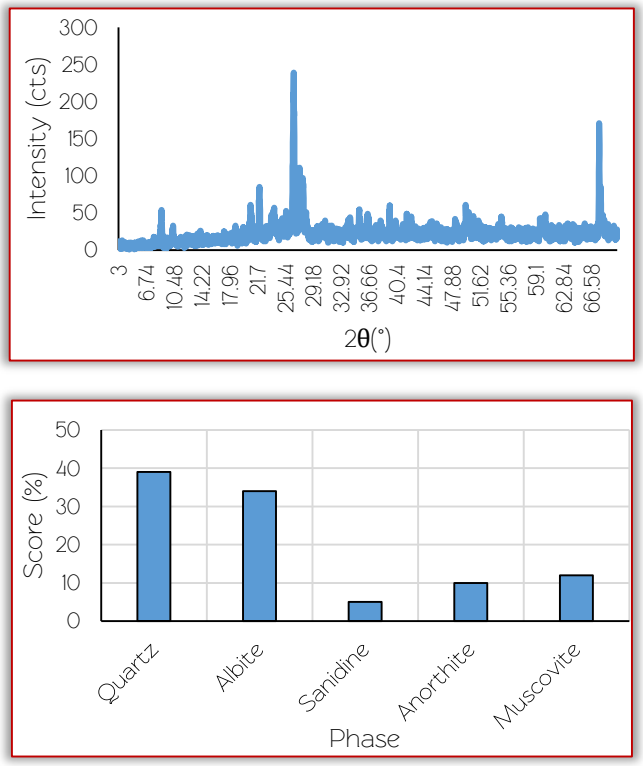

Figure 18. Granite tailings (after leaching): Sample L3–3ML (a) XRD pattern and (b) phases and their scores

After leaching with 5 M HCl, the XRD pattern (Figures 19 (a) and 19 (b)) showed a further shift in phase distribution, with: Quartz emerging more strongly, the appearance of microcline [$KAlSi_3O_8$], a triclinic feldspar, persistent anorthite, albite, and muscovite, and the emergence of topaz [$Al_2SiO_4(F,OH)_2$], a fluorine-bearing aluminosilicate.

Despite stronger acid treatment, the residue still contained several silicate phases. The introduction of topaz, a typically acid-resistant mineral, suggests secondary crystallization or transformation of residual Al and Si under elevated acidity. The diverse phase composition indicates that, although feldspar breakdown continued, the system did not fully simplify; instead, new phases emerged, while muscovite and anorthite remained stable.

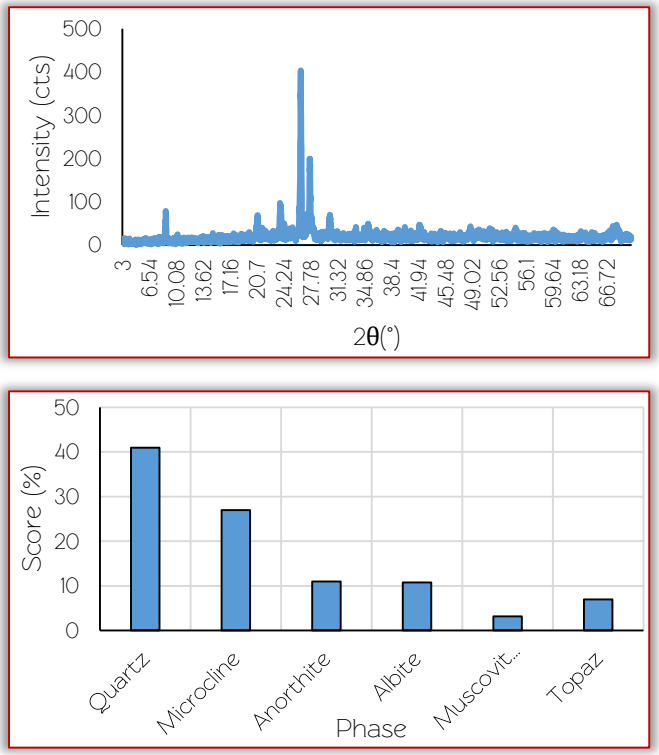

Figure 19. Granite tailings (after leaching): Sample L3–5ML (a) XRD pattern and (b) phases and their scores

Leaching with 7 M HCl resulted in the mineral assemblage changing slightly again (Figures 20 (a) and 20 (b)), showing: Dominance of quartz, with visibly sharper and more intense peaks, continued presence of albite, sanidine, and anorthite, and introduction of biotite-1M [$(K(Mg,Fe)_3AlSi_3O_{10}(OH)_2)$], a dark mica rich in Fe and Mg. The replacement of muscovite with biotite suggests a reorganization or transformation of layered aluminosilicates, potentially involving the mobilization of Fe and Mg (confirmed by EDX) into new mica structures.

Quartz became the most prominent phase, however, the sample remained mineralogically complex, lacking the phase purity observed in L2.

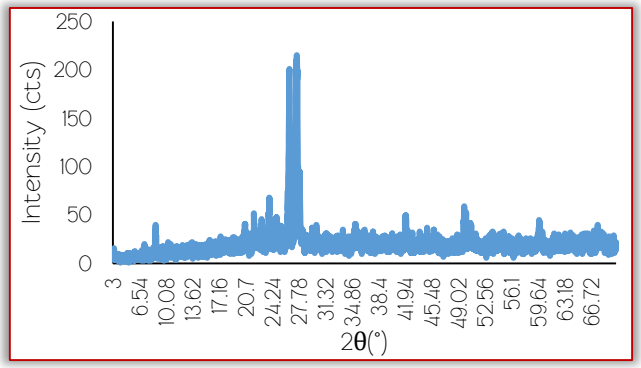

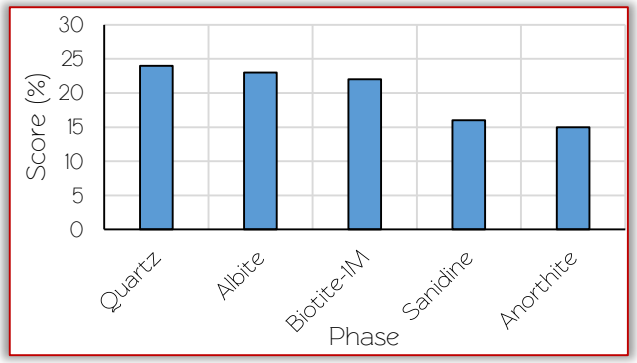

Figure 20. Granite tailings (after leaching): Sample L3–7ML (a) XRD pattern and (b) phases and their scores

Correlation Between Mineralogical Transformations and Silica Purification

SEM and XRD results show that silica enrichment increases as feldspars, clays, and Fe-bearing phases dissolve. L1 and L2 exhibit major loss of orthoclase, albite, muscovite, illite, and montmorillonite, leading to higher post-leaching Si contents, whereas the persistence of mica and feldspar in L3 limits enrichment. The appearance of anorthite at 5 M HCl in L1 and L2 indicates that Ca-Al silicates act as intermediate-resistance phases that dissolve only at higher acidity (7 M), allowing quartz to dominate. Overall, silica purification results from the selective dissolution of Al-, K-, Ca- and Fe-bearing silicates.

CONCLUSIONS

This study investigated the acid leaching behavior of granite tailings from three Nigerian mine sites using HCl at varying concentrations. The characterizations were carried out by SEM-EDX and XRD analyses. The results revealed different responses of the mine tailings obtained from the 3 locations. L1 tailing samples showed optimal silica enrichment at 5 M HCl. However, anorthite dominance was observed at 7 M HCl, which may be due to recrystallization or selective phase retention. L2 tailing samples exhibited strong acid reactivity, and significant impurity removal. At 5 M HCl, anorthite was dominant, while quartz dominance was achieved at 7 M HCl, indicating delayed silica purification. In contrast, L3 tailing samples did not respond effectively to acid leaching. They retained complex feldspar and mica phases across all treatments. Only moderate quartz enrichment was achieved. These findings suggest the need to tailor leaching conditions to the specific mineralogy of granite tailings from different locations for effective silica recovery. Potential applications of the recovered materials are as construction fillers and in ceramics industry. Further research will focus on increasing the silica percentage in the recovered materials by exploring different leaching protocols to meet the requirements for the construction, ceramic and glass making industries.

References

[1] Amin, M., Sumardi, S., Marjunus, R., Clarasati, F., Birawidha, D. C., Muttaqqi, M. A., Isnugroho, K., & Hendronursito, Y. (2020). Processing of granite quarry solid waste into industrial high silica materials using leaching process with HCl concentration variation. Jurnal Riset Teknologi Pencegahan Pencemaran Industri, 11, 43–50

[2] Chen, L., Li, Q., & Jiang, T. (2022). Comprehensive utilization of tailings in quartz vein–hosted gold deposits. Minerals, 12, 1481

[3] Fatoye, A. O. (2022). Geochemical characteristics of unexplored mine tailings in Ijero Ekiti, Nigeria. GSC Advances in Research and Reviews, 11, 57–60.

[4] Hao, X., Zhu, Q., Li, D., Zhang, B., Wang, W., & Wang, A. (2024). Utilization of granite tailings: Dry alkaline thermal activation and novel applications as cementitious materials. Journal of Building Engineering, 88, 109195

[5] Lashen, T. A., Mohamed, S. A., Cheira, M. F., Zaki, D. I., & Allam, E. M. (2016). Leaching and recovery of rare earth elements from altered alkaline granite rock from Nusab El–Balgum area, south–western desert, Egypt. International Journal of Advanced Research, 4, 787–801

[6] Li, C., Tang, X., Liu, X., & Li, S. (2024). Hematite tailings to high–purity silica: Mechanistic studies and life cycle assessment analysis. Chemosphere, 365, 143335.

[7] Li, Y., Li, S., Pan, X., Zhao, X., Guo, P. (2023). Separation and purification of high–purity quartz from high–silicon iron ore tailing. Process Safety and Environmental Protection, 169, 142–148

[8] Li, Y., Li, S., Pan, X., Zhao, X., Guo, P., & Zhao, Z. (2023). Recovery and preparation of high–grade silica from iron ore tailings. Powder Technology, 424, 118523.

[9] Long, H., Xu, X., Li, S., Zhu, D., Pan, J., & Guo, Z. (2025). Utilization of high–silicon iron ore tailings for 4N8 high–purity quartz powder production via two–stage acid leaching. Inorganic Chemistry, 64, 3805–3823

[10] Oyinloye, A. O., & Obasi, R. (2006). Geology, geochemistry and geotectonic setting of the Pan–African granites and charnockites around Ado–Ekiti, southwestern Nigeria. Pakistan Journal of Scientific and Industrial Research, 49, 299–308

[11] Salinas–Rodriguez, E., Flores–Badillo, J., Hernandez–Avila, J., Cerecedo–Saenz, E., Gutierrez–Amador, M. D., Jeldres, R. I., & Toro, N. (2020). Assessment of silica recovery from metallurgical mining waste by means of column flotation. Metals, 10, 72

[12] Yang, S., Han, S., Chen, J., Wei, K., & Ma, W. (2024). A sustainable mineral process for silicon and quartz recovery from quartz crucible waste ash via electrical separation. Minerals Engineering, 216, 108887

[13] Yang, S., Han, S., Wan, H., Wei, K., & Ma, W. (2024). Silicon and quartz recovery and purification from waste quartz crucible ash. Silicon, 16, 4025–4035

[14] Zhang, B., Zhang, H., Xu, R., Wang, L., & Tang, H. (2024). Research on resource comprehensive utilization of granite–type sulfide mine tailings. Journal of Physics: Conference Series

[15] Zhang, R., Tang, C., Ni, W., Yuan, J., Zhou, Y., & Liu, X. (2023). Research status and challenges of high–purity quartz processing technology from a mineralogical perspective in China. Minerals, 13, 1505

ISSN: 2067–3809